Acoustic phonon generation and detection in GaAs/Al$_{0.3}$Ga$_{0.7}$As quantum wells with picosecond laser pulses

O. Matsuda* and T. Tachizaki

Department of Applied Physics, Graduate School of Engineering, Hokkaido University, Sapporo 060-8628, Japan

T. Fukui

Research Center for Integrated Quantum Electronics, Hokkaido University, Sapporo 060-8628, Japan

J. J. Baumberg

Department of Physics and Astronomy, University of Southampton, Southampton SO17 1BJ, United Kingdom

O. B. Wright

Department of Applied Physics, Graduate School of Engineering, Hokkaido University, Sapporo 060-8628, Japan

Picosecond acoustic-phonon pulse generation and detection is investigated in a sample containing three GaAs/Al$_{0.3}$Ga$_{0.7}$As quantum wells of different thickness with an interferometric optical pump and probe technique. The pump photon energy is tuned through the $hh1$-$e1$ transitions of each well and the probe photon energy is chosen to allow the detection of the phonon pulses at the sample surface. The phonon pulse shapes are explained with a model that relates the carrier wave functions to the acoustic strain, and the acoustic strain to the detected optical reflectance and phase changes.

I. INTRODUCTION

Acoustic phonon generation and propagation at frequencies up to the terahertz range can be investigated by exciting and probing solids with ultrashort optical pulses.[1–4] The absorbed pump light pulses generate longitudinal acoustic phonon pulses whose shape is governed by electron relaxation and diffusion, the electron-phonon interaction, thermal diffusion or piezoelectric effects.[5] The propagating phonons are often detected through photoelastically induced changes in reflectivity or transmissivity of delayed probe light pulses or through optical phase shifts caused by surface or interface displacements. This method, known as laser picosecond acoustics, has been applied to a wide variety of metallic and semiconductor films and nanostructures.

The method is not only useful for probing phonon propagation but also for elucidating phonon generation mechanisms dependent on the electron dynamics appropriate to relevant ultrashort time scales and nanometer length scales in solids. In the noble metals or in gallium arsenide, for example, the spatial distribution of the excited electrons has been shown to be effectively imprinted on the phonon strain pulse shape.[2,6] This strain pulse shape can be determined by monitoring the transient surface displacement through interferometric detection or probe beam deflection.[7] Buried semiconductor quantum wells have also been investigated to elucidate the basic physics of phonon generation in confined quantum geometries,[4,8–10] such generation being related to the shape of the electron and hole wave functions and to the strength of the electron-phonon interaction. Preliminary results show that picosecond acoustic phonon pulses can be generated in quantum wells and detected at the sample surface.[4,9] Moreover, the phonon pulses can be excited selectively in the wells by tuning the optical wavelength.[10] Approximate theoretical treatments using simplified models of the wave function shapes were presented to explain the observed phonon pulse shapes.

In this paper we describe the use of a two-color interferometric pump and probe technique with surface probing for the detailed study of picosecond acoustic phonon pulse generation and detection in a triple GaAs/Al$_{0.3}$Ga$_{0.7}$As quantum well structure, and show how the phonon generation region for the three wells depends on the pump optical wavelength. We analyze the results with a rigorous quantum mechanical model taking proper account of the detailed form of the electron and hole wave functions and the optical multiple reflections in the sample. We show how the subject of picosecond acoustics in quantum wells can be put on a quantitative footing, thus opening the way to the use of such structures as well-characterized high frequency phonon transducers in terahertz phonon spectroscopic studies.

In Sec. II we describe briefly the phenomenological classical and quantum-mechanical theories of the optical generation of acoustic waves in semiconductors, with particular application to generation in quantum wells. In Sec. III we present the experimental technique and results and in Sec. IV we describe the theoretical fits and interpretation. The theory for the acoustic wave detection is also given briefly in Sec. IV. Conclusions are then given in Sec. V.

II. THEORY

A. Classical theory of acoustic wave generation in semiconductors by ultrashort light pulses

In this section we outline a simplified phenomenological classical theory of longitudinal acoustic wave generation in

semiconductors with ultrashort light pulses, ignoring piezo-electric effects, with particular reference to generation in a quantum well.[31] We restrict the discussion to amorphous semiconductors or to cubic semiconductor crystals cut in symmetry directions for which an isotropic theory of the acoustic generation is valid.

Before presenting a quantitative model, we shall first qualitatively outline the origins of electronic and thermal stress in semiconductors on optical illumination.[1] Suppose a volume of semiconductor is irradiated with a subpicosecond light pulse with above-band-gap photon energy $E > E_g$. The process of excitation of electrons and holes is maintained throughout the duration of the light pulse and they remain in the conduction and valence bands typically for several nanoseconds or longer. This excitation changes the equilibrium lattice spacing—introducing an electronic stress—because the valence band electrons in general help to bind the lattice more effectively than the conduction electrons (in particular for near-zone-center excitations in direct-gap semiconductors). This coupling between the excited carriers and strain is governed by the deformation potential, which links applied strain to changes in band energies or, conversely, describes the stress in the lattice from excited electron-hole pairs.[11]

After their initial excitation the electrons and holes emit their excess energy to the lattice phonon bath in order to relax down to the conduction and valence band edges. Consider the example of direct-gap polar semiconductors such as GaAs,[12–14] of direct concern in the present paper. If the carrier excess energies are less than the energy of one LO phonon above the band edge, decay to acoustic phonons is expected to be slow (>100 ps). If the carrier excess energies are greater than that of one LO phonon, LO phonon emission is enabled, thus resulting in rapid decay to acoustic phonons (in a few ps). This produces a temperature rise $T - T_0$ (where T_0 is the initial temperature), resulting in a thermal stress.

Including these two stress contributions, the component of the stress tensor σ'_{ij} induced by the processes of carrier excitation and relaxation to the band edges is given by

$$\sigma'_{ij} = \frac{\partial E_g}{\partial \eta_{ij}} n_c - 3B\beta(T - T_0)\delta_{ij}, \qquad (1)$$

where n_c is the density of excited carrier pairs, η_{ij} is the corresponding strain tensor component, B is the bulk modulus, and β the linear thermal expansion coefficient.[32]

Consider the case of a sample with one plane surface irradiated by light from the medium outside it. Provided that the diameter of the irradiated region (typically greater than 1 μm) of the sample is much larger than the irradiated depth, for short time scale measurements (typically less than 1 ns) the excited carrier density and the temperature rise can be assumed to depend only on z, where z is the coordinate axis perpendicular to the sample surface (pointing into the sample). The dominant strain component in this case is η_{zz} owing to the assumed geometry of the system. The appropriate elastic wave equation is one-dimensional:

$$\rho \frac{\partial^2 u_z}{\partial t^2} = \frac{\partial \sigma_{zz}}{\partial z}, \qquad (2)$$

$$\sigma_{zz} = \rho v^2 \eta_{zz} + \frac{\partial E_g}{\partial \eta_{zz}} n_c - 3B\beta(T - T_0), \qquad (3)$$

where $u_z = u_z(z,t)$ is the z component of the elastic displacement, ρ the mass density, and v the longitudinal sound velocity. Here n_c and T are assumed to be functions of z and t.

In general the density of excited electrons and holes may have a different spatial distribution and temporal variation, $n_e(z,t)$ and $n_h(z,t)$, respectively, even though they are initially optically generated in any given volume element in equal numbers n_c. Equation (3) should therefore be replaced with

$$\sigma_{zz} = \rho v^2 \eta_{zz} + \frac{\partial E_c}{\partial \eta_{zz}} n_e - \frac{\partial E_v}{\partial \eta_{zz}} n_h - 3B\beta(T - T_0), \qquad (4)$$

where $\partial E_c / \partial \eta_{zz}$ and $\partial E_v / \partial \eta_{zz}$ are the hydrostatic deformation potentials for the conduction and valence band, respectively. The following relation holds:

$$\frac{\partial E_g}{\partial \eta_{zz}} = \frac{\partial E_c}{\partial \eta_{zz}} - \frac{\partial E_v}{\partial \eta_{zz}}.$$

The deformation potential for the valence band $\partial E_v / \partial \eta_{zz}$ is subtracted since we are considering the energy of holes.

The above treatment is also applicable to generation in a quantum well provided that the distributions $T(z,t)$, $n_e(z,t)$, and $n_h(z,t)$, acting as acoustic source terms, are known. The latter two distributions can only be properly calculated with a quantum-mechanical treatment of the well wave functions. Although we have only considered a model with a single band gap, extension of this treatment to the case of multiple valley excitation is possible.

A variety of specific solutions to the elastic wave equations for known source terms have been obtained.[1,2,5,15–17] In the next section we shall justify the validity of the source terms in Eq. (4) by quantum mechanical arguments.

B. Quantum theory of acoustic wave generation in quantum wells by ultrashort light pulses

The classical theory of strain generation when supplemented by a knowledge of the quantum well wave functions suffices to calculate the acoustic phonon pulses generated therein by ultrashort optical pulses. However, it is instructive to verify this semiclassical result by a rigorous quantum treatment of the acoustic phonon generation in a semiconductor.[18] In this treatment we shall focus in particular on the relation between the phonon and electron wave functions.

In accordance with our assumptions about the symmetry and geometry of the generation region, consider a one-dimensional elastic continuum field of length L and a one-dimensional one-electron Schrödinger field with a square

well potential. The width of the well is assumed to be much smaller than L. These two fields interact with each other through the deformation potential. The system is taken to be elastically homogeneous, a reasonable assumption for the case of the quantum wells used in this study. The thermal stress is taken to be zero at first.

The elastic field is subject to the wave equation

$$\rho\frac{\partial^2 q}{\partial t^2} = C\frac{\partial^2 q}{\partial z^2} + \frac{\partial}{\partial z}(A\psi^*\psi),\qquad(5)$$

where $q(z,t)$ is the elastic displacement, ρ the mass density, C the appropriate elastic modulus, A the deformation potential, and $\psi(z,t)$ the electron wave function which is normalized in three-dimensional space. The sound velocity v is related to C through $C=\rho v^2$. The one-electron Schrödinger equation can be written as follows:

$$\left(-\frac{\hbar^2}{2m}\frac{\partial^2}{\partial z^2} + V(z) + A\frac{\partial q}{\partial z}\right)\psi = i\hbar\frac{\partial\psi}{\partial t}\qquad(6)$$

where m is the electron mass and $V(z)$ represents the square well potential.

As explained in Appendix A, second quantization of the elastic and electron fields yields the total Hamiltonian of the system:

$$\mathcal{H} = \sum_j E_j a_j^\dagger a_j + \sum_k \hbar\omega_k b_k^\dagger b_k$$
$$+ \sum_{j,j',k} \hbar\omega_k(g_{jj'k}b_k a_j^\dagger a_{j'} + g_{jj'-k}b_k^\dagger a_j^\dagger a_{j'}),\qquad(7)$$

where E_j is the energy eigenvalue of the jth state in Eq. (6) with $A=0$, and $\omega_k=v|k|$ is the angular frequency of the elastic wave with wave number k in Eq. (5) with $A=0$. The annihilation and creation operators for the jth electronic state are a_j and $a_j^\dagger$. The operators b_k and $b_k^\dagger$ are those for phonons with wave number k. The coefficient $g_{jj'k}$, arising from the electron-phonon interaction, is defined as

$$\hbar\omega_k g_{jj'k} \equiv ikA\sqrt{\frac{\hbar}{2\rho\omega_k L}}\int \phi_j^*(z)\phi_{j'}(z)e^{ikz}\,dz,$$

where ϕ_j is the wave function of the jth electronic state. It satisfies

$$g_{jj'-k} = g_{jj'k}^*,$$

since the wave function ϕ_j for a square well potential is real.[19]

The electron states arising from the Hamiltonian (7) are well approximated by the eigenstates of a noninteracting electron system if the energy difference between the electron eigenstates E_i-E_j of interest is much larger than the phonon energy $\hbar\omega_k$. This is valid in our experiment: in a GaAs/Al$_{0.3}$Ga$_{0.7}$As single quantum well of width of 7.6 nm, for example, the energy difference between the $e1$ and $e2$

levels is more than 100 meV. This is much larger than the relevant phonon energy of about 4 meV at 1 THz.

Consider the instantaneous excitation of an electron by an ultrashort light pulse into the jth eigenstate at $t=0$. We assume the electron stays in the excited state for $t>0$. This situation can be described by

$$\Phi = \begin{cases} \Phi_l & (t<0) \\ a_j^\dagger\Phi_l & (t\geq 0), \end{cases}$$

where Φ is the complete solution of the equation

$$\mathcal{H}\Phi = i\hbar\frac{\partial\Phi}{\partial t},$$

and Φ_l is the phonon-related part of the solution, that satisfies

$$\mathcal{H}_l\Phi_l = i\hbar\frac{\partial\Phi_l}{\partial t},\qquad(8)$$

where

$$\mathcal{H}_l = \begin{cases} \sum_k \hbar\omega_k b_k^\dagger b_k & (t<0) \\ \sum_k \hbar\omega_k(b_k^\dagger b_k + g_{jjk}b_k + g_{jjk}^* b_k^\dagger) & (t\geq 0). \end{cases}$$

Suppose that the phonon system at $t<0$ is in the ground state Φ_{00} that satisfies $b_k\Phi_{00}=0$ for any k. The state Φ_{00} should thus be taken as the initial condition for Eq. (8) for $t\geq 0$. This is the displaced Bose operator problem and results in the coherent phonon state. The phonon state at $t\geq 0$ is given by

$$\Phi_l = \Pi_k U_k\Phi_0,$$

$$U_k \equiv e^{-(1/2)|g_{jjk}|^2}e^{g_{jjk}^* e^{-i\omega_k t}\tilde{b}_k^\dagger}e^{-g_{jjk}e^{i\omega_k t}\tilde{b}_k},\qquad(9)$$

where Φ_0 is the ground state for $\mathcal{H}_l$ for $t>0$. The annihilation and creation operators with the overtilde are defined using

$$b_k = \tilde{b}_k - g_{jjk}^*,$$

$$b_k^\dagger = \tilde{b}_k^\dagger - g_{jjk}.\qquad(10)$$

Φ_0 is defined to satisfy $\tilde{b}_k\Phi_0=0$ for any k. The operator U_k is chosen to be unitary, and gives unitary conversion of operators $\tilde{b}_k$ and $\tilde{b}_k^\dagger$:

$$U_k^\dagger\tilde{b}_k U_k = \tilde{b}_k + g_{jjk}^* e^{-i\omega_k t},$$

$$U_k^\dagger\tilde{b}_k^\dagger U_k = \tilde{b}_k^\dagger + g_{jjk}e^{-i\omega_k t}.\qquad(11)$$

The operator for strain is given by

$$\frac{\partial q}{\partial z} = \sum_k ik\sqrt{\frac{\hbar}{2\rho\omega_k L}}(e^{ikz}b_k - e^{-ikz}b_k^\dagger).$$

The expectation value of the strain can be calculated for the phonon state of Eq. (9) using Eqs. (10) and (11):

$$\left\langle \Phi \left| \frac{\partial q}{\partial z} \right| \Phi \right\rangle = \frac{A}{2\rho v^2}$$
$$\times \left(-2|\phi_j(z)|^2 + |\phi_j(z-vt)|^2 + |\phi_j(z+vt)|^2\right). \quad (12)$$

This result is exactly the same as the solution for Eq. (2) with the stress

$$\sigma_{zz} = \rho v^2 \eta_{zz} + A|\phi_j(z)|^2. $$

The second and third terms in the round brackets in Eq. (12) describe the propagating components of the strain. The shape of the strain pulse is the same as that of the square of the modulus of the electron wave function.

If a higher phonon number state $\Phi_l(t<0)$ with phonon number n_k for the phonon with wave number k is instead assumed as the initial condition, where

$$\Phi_l = \Pi_k \frac{1}{\sqrt{n_k!}}(b_k^\dagger)^{n_k}\Phi_{00},$$

a similar argument leads to the same strain expectation value as described in Eq. (12). One can thus conclude that the expectation value is not affected by the details of the initial conditions provided that the initial strain expectation value is zero. For a bath of thermally excited phonons as the initial condition, as in experiment (that is a mixture of phonon number states with random phase), the initial strain expectation value vanishes except for a fluctuation term.

In the above treatment, the detailed nature of the carrier-carrier or carrier-phonon scattering is not included. This simplification is reasonable here because these processes mainly affect the carrier energy and momentum distribution on a subpicosecond timescale for the GaAs quantum wells used in the present experiments, and should not significantly influence the coherent acoustic phonon generation. A more sophisticated treatment is beyond the scope of this paper, but might be necessary for quantum wells thinner than ~ 3 nm for which the generated phonon frequencies significantly exceed 1 THz.

From the above we can conclude that the acoustic phonon generation can be accurately treated by the semiclassical treatment of Sec. II A if the carrier densities are replaced with the corresponding probability densities. For the specific example of a quantum well containing a static distribution of electrons and holes excited to their jth states, Eq. (4) should be modified to

$$\sigma_{zz} = \rho v^2 \eta_{zz} - 3B\beta(T(z,t)-T_0) + \frac{\partial E_c}{\partial \eta_{zz}}N_e|\phi_j^{(e)}(z)|^2$$
$$- \frac{\partial E_v}{\partial \eta_{zz}}N_h|\phi_j^{(h)}(z)|^2, \quad (13)$$

where the superscripts (e) and (h) denote the wave functions for electrons and holes, respectively. The quantities N_e and N_h refer to the respective number of excited carriers in the
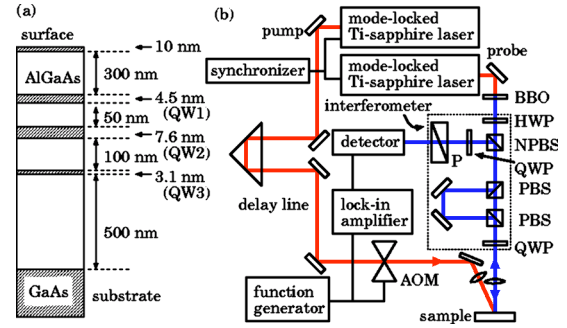

FIG. 1. (Color online) (a) Dimensions of the GaAs/Al$_{0.3}$Ga$_{0.7}$As quantum well structure. (b) Experimental setup. AOM=acousto-optic-modulator, QWP=quarter wave plate, HWP=half wave plate, PBS=polarizing beam splitter, NPBS=nonpolarizing beam splitter, P=polarizer, and BBO=β-BaB$_2$O$_4$ crystal. The region enclosed with a dotted line forms an interferometer.

volume used for the normalization of $\phi_j^{(e,h)}$. (In the case of optical excitation, N_e should be equal to N_h.) The deformation potentials should be treated as position dependent quantities because they differ in general for the barrier and well materials. Equation (13) forms the basis of our analysis of the experimental results in the next section.

III. EXPERIMENT AND RESULTS

A GaAs/Al$_{0.3}$Ga$_{0.7}$As quantum well structure was prepared on a GaAs (100) substrate using MOVPE (metallorganic vapor phase epitaxy). Three buried GaAs quantum wells of different thickness were incorporated in order to exploit their different excitonic optical resonances. The nominal thicknesses and the sample geometry are shown in Fig. 1(a). The calculated $hh1$-$e1$ transition energies at 300 K for the isolated quantum wells labeled QW1, QW2, and QW3 in Fig. 1(a) are 1.55 eV, 1.48 eV, and 1.61 eV, respectively. Photoluminescence measurements at room temperature for this sample show three distinct luminescence peaks near 1.51 eV, 1.46 eV, and 1.56 eV, that are reasonably close to the expected $hh1$-$e1$ transition energies of the three wells.

Figure 1(b) shows a schematic diagram of the experimental setup. Infrared optical pump pulses of photon energy tunable in the range 1.44 eV to 1.68 eV (wavelength 860 nm to 740 nm and spectral bandwidth ~ 3 nm), duration 1.2 ps (full width at half maximum), and repetition rate 82 MHz from a mode-locked picosecond Ti:sapphire laser are used to excite longitudinal acoustic phonon pulses in the quantum wells. In this study we have chosen to enhance the resolution in wavelength at the expense of increased optical pulse duration. The pump photon energy range spans the $hh1$-$e1$ transition of the three wells and is low enough for the pump light to be transmitted by the Al$_{0.3}$Ga$_{0.7}$As barrier layers. The pump light is focused onto the sample surface with a spot radius ~ 20 μm at half maximum intensity, an incident angle of 20°, and an incident fluence ~ 0.05 mJ cm^{-2} per optical pulse. The incident fluence is kept constant while varying the pump photon energy. This fluence typically produces a carrier density in the resonant quantum wells of the order of 10^{12} cm^{-2}, giving rise to a strain amplitude $\sim 10^{-5}$. The sample is placed in a

vacuum cell ($<10^{-4}$ Pa) to avoid oxidation caused by the optical irradiation in air.

The longitudinal acoustic phonon pulses excited inside the sample propagate along the stacking direction, and can be detected at the top surface through the change in reflectance or phase arising from the photoelastic effect or the surface displacement. In contrast to Refs. 2, 4, and 7 in which the bulging associated with the surface displacement is detected by probe beam deflection, here the surface displacement is detected by the change in the phase of the reflected light. A blue probe beam of delayed optical pulses of photon energy 3.06 eV (wavelength 405 nm), spectral width ~5 nm, and duration ~150 fs derived by doubling the light pulses from a second mode-locked femtosecond Ti:sapphire laser synchronized to the first is used to detect the complex reflectance change δr of the sample using a Sagnac interferometer[20] shown in the region of Fig. 1(b) enclosed by the dotted line. The relative reflectance change can be expressed as $\delta r/r = \rho + i\delta\phi$ where ρ and $\delta\phi$ are the real and imaginary parts of the reflectance change. The fluence of the probe pulses is ~2 μJ cm^{-2} and the spot radius is ~15 μm at half maximum intensity. The probe light is normally incident on the sample surface. The time delay between the pump and probe light pulses is scanned from 0 to 400 ps in an optical delay line. Typically 30 scans of the delay line are averaged to obtain a data set. The probe light penetrates about 20 nm into the sample through the cap GaAs layer and part of the adjacent $Al_{0.3}Ga_{0.7}As$ layer. To improve the signal-to-noise ratio, the pump beam is modulated at 1.1 MHz by an acousto-optic modulator, and a lock-in amplifier is used for synchronous detection. All the measurements are done at room temperature.

The transient temperature rise in the quantum wells and in the substrate is of the order of 1 K. The dc temperature rise of the near-surface region of the sample is estimated to be

FIG. 2. (Color online) Calculated relation between the jitter Δt and the output voltage V_{out} of the lock-in amplifier. The inset shows the cross correlation measurement setup that is used for the jitter correction system. F.G.=function generator. BBO=β-BaB$_2$O$_4$ crystal.

<5 K. With these excitation conditions the excitation of acoustic phonon pulses in the sample is expected to be accurately described by a linear theory, and indeed we found that the transient changes in reflectance were proportional to the pump fluence up to the values quoted above.

The maximum raw timing jitter between the light pulses from the two lasers is ~10 ps. In order to compensate for this jitter, a correlation technique is used to correct the timing at each data point in the scan (Fig. 2, inset), using a separate beam line that tracks the jitter between the two lasers. The cross correlation of the infrared light pulses from the two lasers is taken using a BBO (β-BaB$_2$O$_4$) crystal and the frequency-summed light is detected. The detector output is fed to an independent lock-in amplifier; one of the optical path lengths before the BBO crystal is sinusoidally modulated with an amplitude of about ±5 mm, and this modulation (typically at about 10 Hz) is used as the reference input
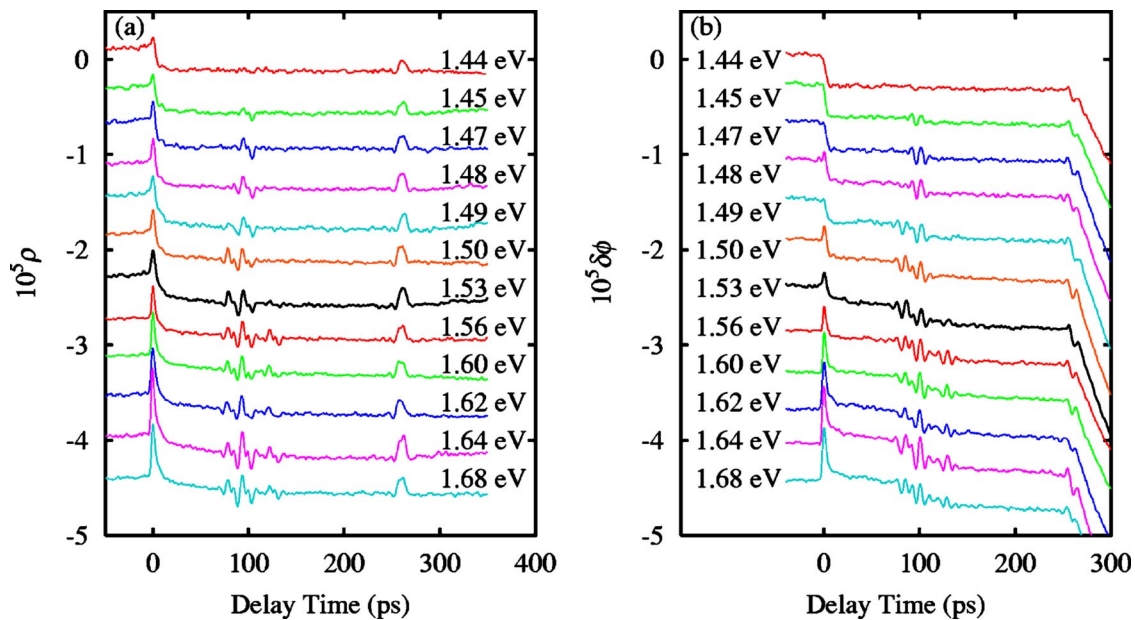

FIG. 3. (Color online) (a) Real and (b) imaginary parts of the complex relative reflectance change $\delta r/r$ at pump photon energies from 1.44 to 1.68 eV in the order from top to bottom. Curves are shifted vertically for clarity.
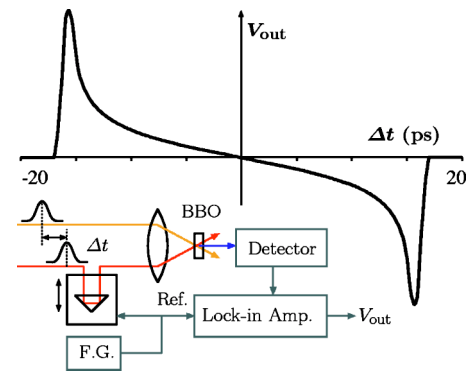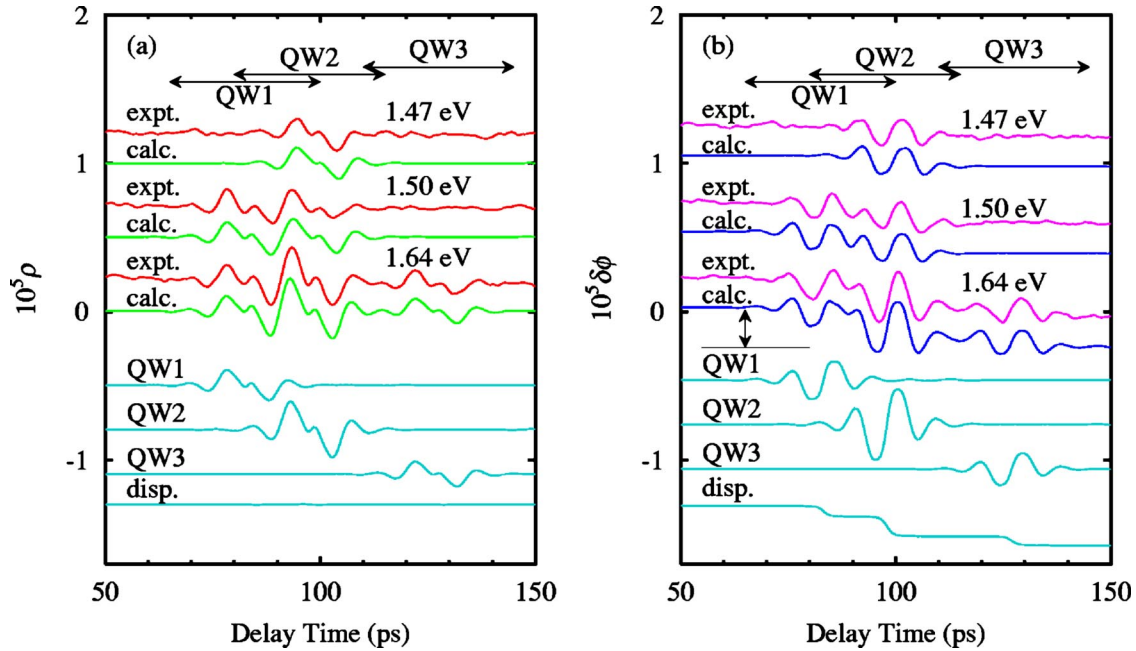
FIG. 4. (Color online) Magnified view of the (a) real and (b) imaginary parts of the complex relative reflectance change $\delta r/r$ at a pump photon energy of 1.47, 1.50, and 1.64 eV. The experimental (expt.) curves and calculated (calc.) curves that are fitted to the data are shown together. The bottom 4 curves show the decomposed photoelastic contributions to the calculated curves for 1.64 eV; curves QW1, QW2, and QW3 correspond to acoustic phonon pulses generated in the respective quantum wells; the contribution from the surface displacement is shown separately (disp.). The horizontal arrows show the temporal regions associated with the contributions to the reflectance from each well. The vertical arrows in the $\delta\phi$ plot denote the change in $\delta\phi$ caused by the surface displacement due to the acoustic phonon pulses generated in the quantum wells for 1.64 eV.

of this lock-in amplifier. The lock-in amplifier output, calculated to be proportional to the jitter in a ±10 ps range (Fig. 2), is recorded during the measurement to correct the temporal axis of the reflectance change after the acquisition of the data. In this way, the effective jitter between pump and probe light pulses is reduced to less than 1 ps.

Results for the real (ρ) and imaginary ($\delta\phi$) parts of the relative reflectance change as a function of delay time are shown in Fig. 3 for various pump photon energies from 1.44 to 1.68 eV. The curves are shifted vertically for clarity. Common features appearing in $\delta\phi$ at delay times >260 ps correspond to the arrival at the surface of phonon pulses generated in the GaAs substrate. The signals at ~100 ps correspond to the arrival at the surface of phonon pulses generated in the quantum wells. The overall duration for this quantum-well signal becomes longer with increasing pump photon energy. This is expected from a consideration of the optical absorption spectra of the wells: the pump energies from 1.45 eV to 1.47 eV should excite phonon pulses only at the well QW2, whereas pump energies higher than 1.53 eV should do so in all the wells. (The well QW2 is the thickest and thus has the lowest $hh1$-$e1$ transition energy.) The energies from 1.49 eV to 1.50 eV allow QW1 and QW2 to be excited. The oscillatory nature of the reflectance changes near 100 ps and near 260 ps is characteristic of the photoelastic effect combined with the effect of optical probe penetration into the sample.[1] The curves labeled "expt." in Fig. 4 represent a magnified view around 100 ps for 1.47, 1.50, and 1.64 eV pump photon energies, corresponding to the excitation of QW2, QW1 +QW2, and QW1+QW2+QW3, respectively. The temporal

regions associated with the contribution from each quantum well are indicated by the horizontal arrows. Also noticeable is the downward step in $\delta\phi$ that occurs after the reflection of the phonon pulses from the surface near 100 ps time delay (indicated by the vertical arrows in the $\delta\phi$ graph of Fig. 4 for the case of 1.64 eV), implying a net outward displacement of the sample surface: the total change ~10^{-6} in $\delta\phi$ corresponds to a displacement of ~0.03 pm. This step is the signature of unipolar phonon pulses, as expected and as previously observed in such buried quantum well structures.[9,10]

The fast changes in ρ and $\delta\phi$ around 0 ps show a strong pump-photon energy dependence. This can be attributed to the relaxation of electrons excited in the GaAs cap layer and to the accompanying temperature change.[14]

IV. DISCUSSION

In order to interpret the experimental data further, we have performed a simulation that takes into account the phonon generation, propagation, and detection processes.

A. Phonon generation

The absorbed photons set up an excited carrier distribution. As described in Sec. II the acoustic strain is generated by this carrier distribution through the deformation potential as well as by the temperature rise that is caused by the relaxation of excited carriers towards the conduction and valence band edges.[1,5,6,21]

TABLE I. Refractive indices of each layer for the pump light. Apart from the extinction coefficients K for the GaAs cap and well layers, the values are taken from Ref. 22. The quantity d represents the layer thickness (nm).

Layer	Photon energy (eV)		
	1.47	1.50	1.64
$Al_{0.3}Ga_{0.7}As$	3.40	3.41	3.48
GaAs cap ($d=14$)	$3.65+0.01i$	$3.67+0.01i$	$3.72+0.01i$
QW1 ($d=4.5$)	3.65	$3.67+0.06i$	$3.72+0.09i$
QW2 ($d=7.6$)	$3.65+0.02i$	$3.67+0.04i$	$3.72+0.10i$
QW3 ($d=3.1$)	3.65	3.67	$3.72+0.12i$
GaAs substrate	$3.65+0.04i$	$3.67+0.06i$	$3.72+0.11i$

In order to estimate the quantity $N_e=N_h$ in Eq. (13), we make a preliminary calculation of the absorbed pump photon distribution using the refractive indices and thicknesses quoted in Table I. For this estimate we assume that the quantum wells can be characterized by a uniform dielectric constant. The pump light pulses are assumed to have a Gaussian temporal shape with a full width at half maximum duration of 1.2 ps. The pump-energy dependent (effective) extinction coefficients K for each GaAs well and for the cap layer are adjusted to fit the data whereas the optical constants for the other layers are taken from the literature.[22] The thicknesses of the barrier layers are also adjusted. Details of general fitting procedure are described later. A standard transfer-matrix method is used to deal with the multiple reflection of the pump light in the structure, allowing the relative energy absorption in the parts of the structure with finite extinction coefficient to be evaluated (as described in Ref. 23 and references therein). The absorbed photon number per pump light pulse in each well is equated to the number of excited electrons and holes in the well in question. The corresponding carrier densities are then evaluated and used to calculate the acoustic phonon generation from Eq. (13). The approximately homogeneous distribution of absorbed pump light energy in the quantum wells obtained from the above estimates is not used in the following analysis. Rather we take into account the quantum-mechanical wave functions in the wells.

For our choices of well thickness the quantum wells can be characterized using the envelope function approximation.[19,26] For simplicity we ignore the effect of band mixing; a square well potential is assumed for the conduction electrons, light holes, and heavy holes independently in the Schrödinger equation for the envelope function

$$\left\{-\frac{\hbar^2}{2m_\mu(z)}\frac{d^2}{dz^2}+V_\mu(z)\right\}\phi_{j,\mu}=E_{j,\mu}\phi_{j,\mu}, \qquad (14)$$

where the suffix μ specifies the particle types: electron, heavy hole, and light hole. The band gap energy and conduction band offset (the ratio $\Delta E_c/\Delta E_g$ where ΔE_c is the energy difference in the conduction band minimum and ΔE_g is the difference in the energy gap between barrier and well mate-

rials) are given in Table II.[24,27,28] The effective masses are chosen to be those of bulk GaAs and $Al_{0.3}Ga_{0.7}As$ ignoring any effects of band nonparabolicity. At the $GaAs/Al_{0.3}Ga_{0.7}As$ interface the continuity of $\phi_{j,\mu}$ and $1/m_\mu \cdot d\phi_{j,\mu}/dz$ are imposed as boundary conditions for the wave function envelope. As an example the electron and heavy hole wave functions for a quantum well of thickness 3 nm, similar to QW3, calculated using the parameters of Table II are shown in Figs. 5(a) and 5(b). Some penetration of the wave functions into the barrier layers is evident.

The previous result, Eq. (13), for phonon generation can be applied to the envelope function. The elastic stress is coupled to the carrier densities through the deformation potentials $dE_{c,v}/d\eta_{zz}$ for the conduction and valence bands in the vicinity of the Γ point. These deformation potentials are given in Table II. The positive value of $dE_v/d\eta_{zz}$ implies that the energy of electrons (holes) in the valence band rises (falls) on expansion. The thermal stress $\sigma_{zz,th}$ can be calculated from the equation

$$\sigma_{zz,th}=-3B\beta n_p\frac{h\nu_p-E_g}{C_V}, \qquad (15)$$

where n_p is the density of absorbed pump photons, C_V is the isovolumic heat capacity per unit volume, and $h\nu_p$ is the pump photon energy. In the present experiments, however, we estimate the thermal stress to be ~ 0.03 of the electronic stress at most (for 1.68 eV pump), and it therefore gives a negligible contribution to the strain generation. The effect of thermal diffusion, neglected in this estimate, only serves to smear out this contribution. Figure 5(c) shows the calculated strain profile in QW3. The profile is made up of a combination of electron and heavy hole contributions and has a spatial extent similar to that of the quantum well width. We assume all the holes are accommodated in the heavy hole band for simplicity. (If instead populations are assumed on both the heavy and light hole bands the changes to the calculated strain pulse are not significant.) The induced (hydrostatic) stress distribution launches longitudinal acoustic phonon strain pulses of exactly the same spatial profile in opposite directions ($\pm z$), according to Eqs. (2) and (13). In the present experiments we only detect the strain pulses that are launched towards the surface. The temporal width of the strain pulse launched from QW3 is about 1 ps. Figure 5(d)

TABLE II. Material parameters used for the simulation. Values are taken from Refs. 22, 24, and 25 except the photoelastic constants which are fitted to the data (see the text) and the value of b for GaAs, which is set to zero.

	GaAs	Al$_{0.3}$Ga$_{0.7}$As
Energy gap, E_g (eV)	1.43	1.83
Conduction band offset $\Delta E_c/\Delta E_g$	0.658	
Electron mass, m_e	0.0635m_0	0.0841m_0
Heavy hole mass, m_{hh}	0.33m_0	0.384m_0
Light hole mass, m_{lh}	0.09m_0	0.117m_0
(m_0: free electron mass)		
Deformation potential for conduction band, $dE_c/d\eta_{zz}$ (eV)	−5.3	−5.39
valence band, $dE_v/d\eta_{zz}$ (eV)	2.7	2.67
Bulk modulus, B (GPa)	75.5	75.6
Linear thermal expansion coefficient, β (10^{-6} K^{-1})	6.1	5.3
Specific heat, C_V/ρ (10^2 J kg^{-1} K^{-1})	3.2	3.6
Longitudinal sound velocity, v (km s^{-1})	4.73	4.95
Mass density, ρ (g cm^{-3})	5.36	4.88
Coefficient for ultrasonic absorption, b (m^{-1} GHz^{-2})	0	35
Refractive index $N+iK$ @ $h\nu$=3.06 eV	4.39+2.16i	4.85+1.56i
Photoelastic constant $\frac{dN}{d\eta}+i\frac{dK}{d\eta}$ @ $h\nu$=3.06 eV		
for Fig. 6 (pump 1.47 eV)	−16.9+7.7i	−1.3+40.4i
for Fig. 7 (pump 1.50 eV)	−15.3+6.5i	−2.9+38.4i
for Fig. 8 (pump 1.64 eV)	−14.8+5.1i	−1.5+41.1i

shows the temporal Fourier transform of this strain pulse, showing that frequency components up to 1 THz are present. This frequency is significantly higher than that obtainable with bulk metallic or semiconductor samples, suggesting the potential for the use of quantum wells as terahertz acoustic transducers.
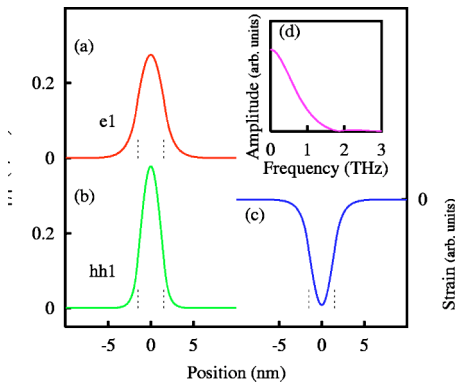

FIG. 5. (Color online) The value of $|\phi|^2$ for the envelope function of (a) the $e1$ electronic state and (b) the $hh1$ heavy hole state for a GaAs/Al$_{0.3}$Ga$_{0.7}$As quantum well of width 3 nm. The excitation of these states with an ultrashort light pulse generates the strain pulse (c) whose frequency spectrum is shown in (d). The dotted lines show the well width.

B. Phonon propagation and detection

The phonon propagation is calculated from the one-dimensional elastic wave equation using the literature values of physical constants shown in Table II. Multiple acoustic reflections are taken into account although their effect is negligible. (The small acoustic impedance mismatch between the GaAs and Al$_{0.3}$Ga$_{0.7}$As layers leads to an acoustic reflection coefficient for strain at the GaAs/Al$_{0.3}$Ga$_{0.7}$As interface of only ∼±0.02.) Frequency-dependent ultrasonic attenuation is included as $\alpha_u=bf^2$ where α_u is the ultrasonic absorption coefficient, f is the ultrasonic frequency, and b is a constant coefficient. A tentative value of b =35 m^{-1} GHz^{-2} is assumed for Al$_{0.3}$Ga$_{0.7}$As, which is not very far from the experimentally obtained value of 12 m^{-1} GHz^{-2} for bulk GaAs.[29] Because the GaAs quantum well and cap layers are so thin, we have set as a simplifying assumption the value of b to zero in GaAs. The fitted reflectance changes are not very sensitive to the exact values of b taken. (As an example of the effect of the ultrasonic attenuation, the duration of the phonon pulse from QW3, the thinnest well, is broadened by a factor of ∼3 by the time this pulse arrives at the sample surface.)

The traveling acoustic phonon pulses modulate the optical properties of the sample inhomogeneously through the photoelastic effect and also displace the surface and interfaces of

the sample. The inhomogeneous perturbation relevant to the blue probe light ($h\nu = 3.06$ eV) reflection here resides in the GaAs cap layer and in the adjacent $Al_{0.3}Ga_{0.7}As$ barrier layer. The complex reflectance change caused by these perturbations can be calculated by a general method including the effect of multiple optical reflections of the probe light inside the structure.[23]

Defining the complex dielectric constant of the GaAs cap layer of thickness h as ε_1 and that of the barrier layer as ε_2, the complex relative reflectance change for this two-layer case is given by

$$\frac{\delta r}{r} = \frac{ik}{2a_0 b_0}\left\{ \int_0^h dz'\, \Delta\varepsilon(z',t)(a_1 e^{ik_1 z'} + b_1 e^{-ik_1 z'})^2 \right.$$

$$+ \int_0^\infty dz'\, \Delta\varepsilon(z'+h,t)a_2^2 e^{2ik_2 z'}$$

$$+ (a_1 + b_1)^2(1-\varepsilon_1)u_z(0,t)$$

$$\left. + a_2^2(\varepsilon_1 - \varepsilon_2)u_z(h,t) \right\}, \qquad (16)$$

with

$$a_0 = (k+k_1)(k_1+k_2) + (k-k_1)(k_1-k_2)e^{2ik_1 h},$$

$$b_0 = (k-k_1)(k_1+k_2) + (k+k_1)(k_1-k_2)e^{2ik_1 h},$$

$$a_1 = 2k(k_1+k_2),$$

$$b_1 = 2k(k_1-k_2)e^{2ik_1 h},$$

$$a_2 = 4kk_1 e^{ik_1 h}.$$

Here k, $k_1 = \sqrt{\varepsilon_1}k$, and $k_2 = \sqrt{\varepsilon_2}k$ are the probe beam optical wave numbers in the air, in the cap layer, and in the barrier layer, respectively. The position of the sample surface is defined as $z=0$ and the sample occupies the positive z region. The changes in dielectric constant for the cap or barrier layers in Eq. (16) are related to the strain through the equation

$$\Delta\varepsilon = 2(N+iK)\left(\frac{dN}{d\eta_{zz}} + i\frac{dK}{d\eta_{zz}}\right)\eta_{zz}(z,t), \qquad (17)$$

where N and K are the real and imaginary parts of the refractive index, and $dN/d\eta_{zz}$ and $dK/d\eta_{zz}$ are photoelastic constants. The surface and interface displacements are denoted by $u_z(0,t)$ and $u_z(h,t)$, respectively. The refractive index and dielectric constant are related through the relation $\varepsilon = (n+iK)^2$.

Equation (16) is made up of contributions from both the photoelastic effect and the transient surface and interface displacements. Because of the inhomogeneous refractive index distribution caused by the propagating phonon strain pulse, the probe light reflectance depends on the integral of the photoelastic optical response over the region of probe light penetration into the sample, as evident in Eq. (16). In general the strain field $\eta_{zz}(z,t)$ contains components traveling in both the $+z$ and $-z$ directions because the phonon pulse is re-
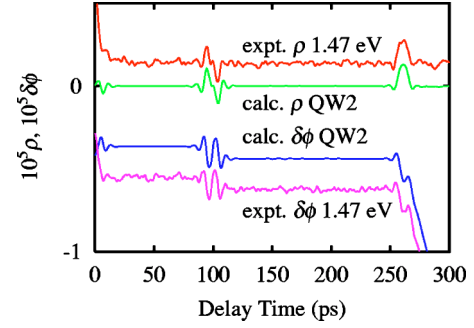

FIG. 6. (Color online) Calculated and experimental curves for the real (ρ) and imaginary ($\delta\phi$) parts of the complex relative reflectance change $\delta r/r$ at pump photon energies 1.47 eV. The scales in each set of four curves are identical.

flected from the surface or cap-barrier interface. The intimate connection between the surface displacement $u_z(0,t)$ and the optical response is also evident in this equation. The effect of the surface displacement, rather than that of the interface displacement $u_z(h,t)$, is dominant because of the much larger optical reflection from the top surface compared to that from the cap-barrier interface. The main effect of the term proportional to $u_z(0,t)$ is therefore to produce an optical phase shift (the downward shift in $\delta\phi$) equal to $2ku_z(0,t)$. The variation $u_z(0,t)$ is related to the acoustic strain distribution in the sample through

$$u_z(0,t) = \int_{+\infty}^0 \eta_{zz}(z',t)dz'.$$

Note that negative $u_z(0)$ corresponds to an outward movement of the surface.

C. Fitting to the experimental results

The set of four curves in Fig. 6, all plotted on the same scale, show data and calculations for ρ and $\delta\phi$ next to one another for the pump photon energy of 1.47 eV. In accordance with the assumed parameters in Table I, only QW2 generates phonon pulses in this case. Full account is taken of the quantum-mechanical predictions for the wave function
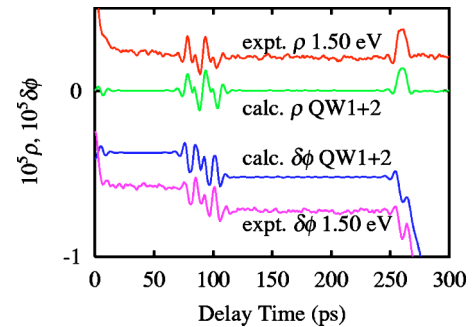

FIG. 7. (Color online) Calculated and experimental curves for the real (ρ) and imaginary ($\delta\phi$) parts of the complex relative reflectance change $\delta r/r$ at pump photon energies 1.50 eV. The scales in each set of four curves are identical.
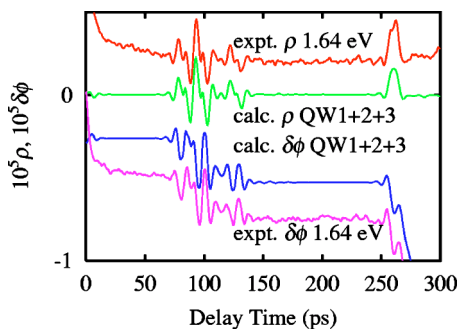
FIG. 8. (Color online) Calculated and experimental curves for the real (ρ) and imaginary ($\delta\phi$) parts of the complex relative reflectance change $\delta r/r$ at pump photon energies 1.64 eV. The scales in each set of four curves are identical.

shape. The sets of curves in Figs. 7 and 8 show data and calculations for the pump photon energies 1.50 eV and 1.64 eV, respectively. We assume that both QW1 and QW2 generate phonon pulses in the calculation for 1.50 eV, whereas all three wells generate phonon pulses in the calculation for 1.64 eV. In all cases the relative carrier densities in the wells are calculated using the parameters in Table I.[33] The comparison between the experimental data and the theoretical predictions is magnified in Fig. 4. The overall agreement is very good.

To clarify the origin of the signals, we show the decomposed contributions for 1.64 eV pump photon energy in the bottom four curves of Fig. 4. The curves labeled QW1, QW2, and QW3 represent the photoelastic contributions from acoustic phonon pulses generated in the respective quantum wells, whereas the curve labeled "disp." represents the variation in the surface displacement.

The fitting procedure involves the adjustment of the extinction coefficients K of each GaAs layer except the substrate, the thicknesses of each layer, and the photoelastic constants ($dN/d\eta_{zz}+idK/d\eta_{zz}$) of the cap and barrier layers using the method of least squares.

The extinction coefficients K of the well layers are largely determined by the ratio between the surface displacements caused by the phonon pulses generated in the quantum wells (producing the downward steps in $\delta\phi$) and those caused by the phonon pulses generated in the GaAs substrate (producing the steadily falling $\delta\phi$ at times greater than 260 ps). However, the oscillatory components of ρ and $\delta\phi$, which arise from the photoelastic effect when the phonon pulses arrive at the sample surface, also facilitate the determination of the values of K because the amplitude of these components are approximately proportional to the area of the strain pulse. This can be seen from Eqs. (16) and (17) for the case in which the strain pulses are small compared to the probe optical absorption depth ($\sim$20 nm), as in this experiment. Fitting to the data for a range of wavelengths gives a spectrum for K for each well, as shown in Fig. 9. We have assumed that clear onsets of the absorption occur in the order QW2, QW1, and QW3 on increasing the photon energy. These assumptions concerning the selective excitation of the phonon pulses as a function of pump wavelength are borne out by the agreement found between the experimental results
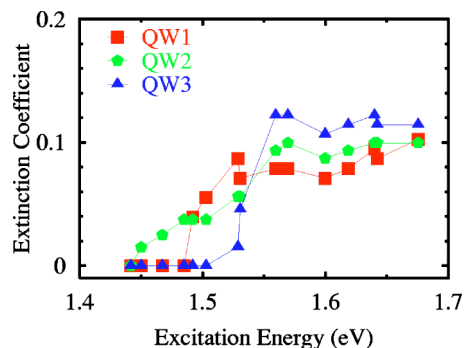

FIG. 9. (Color online) Effective extinction coefficients K for each quantum well deduced from the fitting. The order of the onset from lower to higher energy is QW2, QW1, and QW3 as expected. The lines are guides to the eye.

and the theoretical fits for all the wavelengths studied in Fig. 3 (although we have only presented comparisons for three wavelengths in this paper).

The photoelastic constants as well as the thickness of the cap layer are determined from a simultaneous fit to the oscillatory components in ρ and $\delta\phi$. As shown in Table II, we used slightly different values of the photoelastic constants for each pump photon energy; the overall variation in photoelastic constants used is shown in Fig. 10. As expected, because of the fixed probe wavelength,there is no significant variation with pump photon energy. The photoelastic constant obtained for the GaAs cap layer differs somewhat from the value $-12.1+15.5i$ reported in the literature.[34] This discrepancy may be due to the thinness of the cap layer resulting in carrier confinement or to a high defect concentration near the sample surface.

The net surface displacement caused by each strain pulse arriving at the surface is also a useful parameter to characterize the phonon generation in the quantum wells. The outward surface displacements corresponding to each well calculated from the fitting process are plotted in Fig. 11 as a function of the pump photon energy. The surface displacement is approximately proportional to the product of K and the well width, so thicker wells are expected to generate larger surface displacements. This tendency is observed in Fig. 11, although the signal overlap from adjacent wells de-
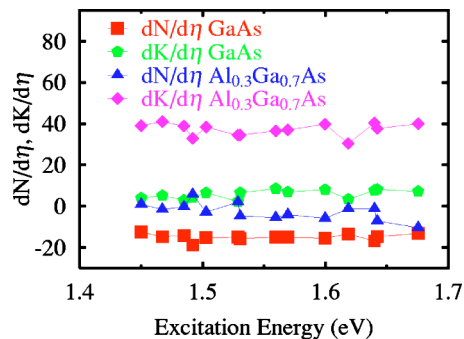

FIG. 10. (Color online) Photoelastic constants for the cap GaAs and adjacent Al$_{0.3}$Ga$_{0.7}$As layers obtained from the fitting for various pump photon energies. They show no apparent pump-photon energy dependence. The lines are guides to the eye.
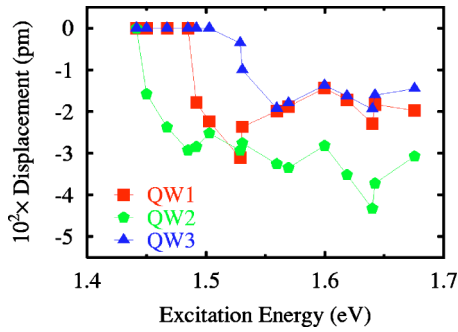
FIG. 11. (Color online) Surface displacement caused by the phonon pulses generated in each quantum well obtained from the fitting for various pump photon energies. The order of the onset from lower to higher energy is QW2, QW1, and QW3 as expected. The lines are guides to the eye.

creases the accuracy of the calculation, particularly for the higher pump photon energies.

The temporal evolution of the surface displacement $u_z(0,t)$ can be obtained from the simulation, as shown in Fig. 4. Figure 12 shows the fitted surface displacement variation separately for the thinnest quantum well QW3 for the pump photon energy of 1.64 eV. The surface velocity $du_z(0,t)/dt$, also shown for the case of 1.64 eV in Fig. 12, is proportional to the strain pulse shape in the present case of a free top surface.[7] The inset of Fig. 12 shows the Fourier transform of $du_z(0,t)/dt$. The width of the frequency spectrum (up to 400 GHz) is considerably narrowed with respect to that (>1 THz) shown in Fig. 5(d). This is due to the frequency dependence of the ultrasonic attenuation in the $Al_{0.3}Ga_{0.7}As$ barrier layers at room temperature. In fact this ultrasonic attenuation essentially removes the high frequency components from the phonon pulses to the extent that the three wells produce phonon pulses with almost identical frequency spectra and strain durations ∼3 ps when detected at the surface.[35]

The cap layer widths quoted in Table I are determined with an accuracy of 1–2 nm, and the barrier thicknesses are determined to an accuracy of a few nanometers. The
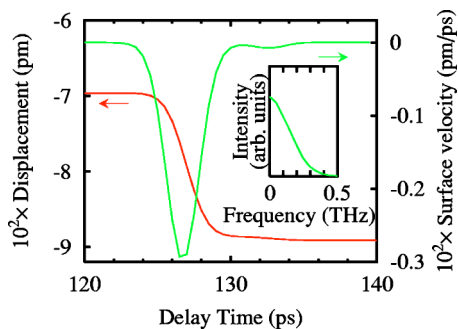

FIG. 12. (Color online) Temporal evolution of the surface displacement (referred to the left axis) and the surface velocity (right axis) both calculated for the pump photon energy of 1.64 eV for the thinnest well QW3. The features around 127 ps corresponds to the arrival at the surface of the acoustic phonon pulse generated in QW3. The inset shows the amplitude of the Fourier transform of the surface velocity.

accuracy in the determination of the quantum well widths is only ∼5 nm, and so we set the well widths equal to the nominal widths estimated from deposition times. This is not enough to evaluate the phonon pulse shape in the generation region and thus the shape of the wave functions. Apart from the effect of the ultrasonic attenuation mentioned above, another reason for this relatively low accuracy is the ∼1 ps pump optical pulse duration corresponding to a spatial smoothing ∼5 nm. One more reason is that the signal due to the surface displacement, directly proportional to the spatial integral of the phonon strain pulse shape, is obscured by the relatively extended oscillatory signal caused by the photoelastic effect. Techniques that allow the discrimination of the photoelastic effect and the surface displacement using polarized oblique probe light incidence[30] together with the use of shorter optical pulse durations and wells positioned nearer to the surface could be exploited in the future to accurately determine the generated phonon strain pulse shape and hence those of the electron and hole wave functions. The use of lower temperatures might help to reduce the phonon pulse broadening caused by ultrasonic attenuation, although temperature-independent alloy scattering in the AlGaAs layers is probably the dominant effect.

V. CONCLUSIONS

We have studied the longitudinal acoustic phonon generation and detection in a $GaAs/Al_{0.3}Ga_{0.7}As$ triple quantum well structure using laser picosecond acoustics. The pump-wavelength dependence of the phonon pulse shapes conclusively demonstrates that we have achieved wavelength-selective phonon excitation in the three quantum wells. The acoustic-phonon pulse generation mechanism is described and treated rigorously with a quantum-mechanical formalism, taking into account the shape of the electron and hole wave function envelopes. The theoretical simulations give good agreement with the experimental results. However, the optical pulse width used is not short enough to clarify the exact shape of the generated acoustic phonon pulses. We also find that the modulated reflectance signals associated with the phonon pulses are dominated by photoelastic effects and are affected by ultrasonic attenuation, thus preventing an accurate determination of the shape of the quantum well wave functions. An improvement of the experimental technique to separate different signal contributions and an optimized sample design should allow this goal to be pursued in the future. However, the present study has shown that it is possible to understand the detailed features of the modulated reflectance arising from the phonon pulses generated in the quantum wells as well as the physics of the generation process. Apart from the fundamental interest in coupling the fields of quantum mechanics and acoustics, this research should lead to interesting developments in high frequency acoustic-optic modulation, in nanoscale acoustic transduction and in terahertz phonon spectroscopy.

APPENDIX A: SECOND QUANTIZATION OF THE ELASTIC WAVE FIELD AND THE ONE-ELECTRON SCHRÖDINGER FIELD

In this appendix we derive the Hamiltonian equation (7) by a standard procedure:[18] (1) determine the interaction between the classical elastic field and the Schrödinger field; (2) find the associated Lagrangian; (3) find the Hamiltonian; and (4) quantize the Hamiltonian (second quantization).

The classical elastic field obeys Eq. (5). The classical electron Schrödinger field (before second quantization of the electron field) obeys Eq. (6) and its complex conjugate that we denote as (6)*. Equations (5) and (6), and (6)* are derived from the following Lagrangian (applied to unit area):

$$\mathcal{L} = \int dz \, \psi^* \left\{ i\hbar \frac{\partial}{\partial t} - V(z) \right.$$
$$\left. + \frac{\hbar^2}{2m} \frac{\partial^2}{\partial z^2} \right\} \psi + \frac{1}{2} \left\{ \rho \left(\frac{\partial q}{\partial t} \right)^2 - C \left(\frac{\partial q}{\partial z} \right)^2 \right\} - A \frac{\partial q}{\partial z} \psi^* \psi, \tag{A1}$$

through the Lagrange's equation of motion for q, ψ, and ψ^*.

The canonically conjugate momenta for q and ψ can be derived from Eq. (A1):

$$\pi_q = \frac{\delta \mathcal{L}}{\delta \dot{q}} = \rho \dot{q}, \tag{A2}$$

$$\pi_\psi = \frac{\delta \mathcal{L}}{\delta \dot{\psi}} = i\hbar \psi^*. \tag{A3}$$

This allows the derivation of the classical Hamiltonian:

$$\mathcal{H} = \int dz (\pi_\psi \dot{\psi} + \pi_q \dot{q} - \mathcal{L})$$
$$= \int dz \, \psi^* \left\{ -\frac{\hbar^2}{2m} \frac{\partial^2}{\partial z^2} + V(z) \right\} \psi + \frac{1}{2\rho} \pi_q^2 + \frac{C}{2} \left(\frac{\partial q}{\partial z} \right)^2$$
$$+ A \frac{\partial q}{\partial z} \psi^* \psi. \tag{A4}$$

Quantization is achieved by replacing the quantities q, π_q, ψ, ψ^* with operators that satisfy the commutation relations,

$$[\pi_q(z), q(z')] = -i\hbar \delta(z - z'), \tag{A5}$$

$$[\pi_\psi(z), \psi(z')]_+ = -i\hbar \delta(z - z'). \tag{A6}$$

The second expression can be rewritten as

$$[\psi(z), \psi^*(z')]_+ = \delta(z - z'). \tag{A7}$$

The suffix $+$ in the commutation relation represents the application to fermions. The remaining sets of operators are commutative:

$$[\psi^*(z), \psi^*(z')]_+ = [\psi(z), \psi(z')]_+ = 0,$$

$$[\pi_q(z), \pi_q(z')] = [q(z), q(z')] = 0,$$

$$[\psi^*(z), q(z')] = [\psi(z), q(z')] = 0,$$

$$[\psi^*(z), \pi_q(z')] = [\psi(z), \pi_q(z')] = 0.$$

The final stage of the analysis consists of expanding the operators ψ, ψ^*, q, π_q with corresponding eigenfunctions for the noninteracting fields. We use the plane wave solution $\exp(ikz)$ with wave vector k for the elastic wave equation:

$$\rho \frac{\partial^2 q}{\partial t^2} = C \frac{\partial^2 q}{\partial z^2}. \tag{A8}$$

For the Schrödinger wave field we use the eigenfunction $\phi_j(z)$ of the one-electron Schrödinger equation:

$$\left(-\frac{\hbar^2}{2m} \frac{\partial^2}{\partial z^2} + V(z) \right) \phi_j = E_j \phi_j. \tag{A9}$$

In addition, we define

$$\psi(z) = \sum_j a_j \phi_j(z), \tag{A10}$$

$$\psi^*(z) = \sum_j a_j^\dagger \phi_j^*(z), \tag{A11}$$

$$q(z) = \sum_k \sqrt{\frac{\hbar}{2\rho \omega_k L}} (e^{ikz} b_k + e^{-ikz} b_k^\dagger), \tag{A12}$$

$$\pi_q(z) = \sum_k i \sqrt{\frac{\hbar \omega_k \rho}{2L}} (-e^{ikz} b_k + e^{-ikz} b_k^\dagger), \tag{A13}$$

where $\omega_k = v|k|$ is the phonon angular frequency. Here a_j and $a_j^\dagger$ are the annihilation and creation operators of the jth electronic state, whereas b_k and $b_k^\dagger$ are those of the phonon state with wave vector k. Substitution into Eq. (A4) yields the Hamiltonian (7). The zero point vibration is removed by an appropriate choice of zero energy. This result is very similar to that for an interacting electron-phonon system with translational symmetry, but here the momentum is not a good quantum number for the electron.

*Electronic address: omatsuda@eng.hokudai.ac.jp

[1] C. Thomsen, H. T. Grahn, H. J. Maris, and J. Tauc, Phys. Rev. B **34**, 4129 (1986).

[2] O. B. Wright, Phys. Rev. B **49**, 9985 (1994).

[3] B. Bonello, B. Perrin, and C. Rossignol, J. Appl. Phys. **83**, 3081 (1998).

[4] J. J. Baumberg, D. A. Williams, and K. Köhler, Phys. Rev. Lett. **78**, 3358 (1997).

[5] V. E. Gusev and A. A. Karabutov, *Laser Optoacoustics* (American Institute of Physics, Woodbury, NY, 1993).

[6] O. B. Wright, B. Perrin, O. Matsuda, and V. E. Gusev, Phys. Rev. B **64**, 081202(R) (2001).

[7] O. B. Wright and K. Kawashima, Phys. Rev. Lett. **69**, 1668 (1992).

[8] K. Mizoguchi, M. Hase, S. Nakashima, and M. Nakayama, Phys. Rev. B **60**, 8262 (1999).

[9] I. Ishii, O. Matsuda, T. Fukui, J. J. Baumberg, and O. B. Wright, in *Proceedings of the 25th International Conference on Physics Semicond., Osaka, 2000*, Springer Proceedings in Physics, edited by N. Miura and T. Ando (Springer-Verlag, Berlin, 2001), No. 87, pp. 871–872.

[10] O. Matsuda, I. Ishii, T. Fukui, J. J. Baumberg, and O. B. Wright, Physica B **316–317**, 205 (2002).

[11] P. Y. Yu and M. Cardona, *Fundamentals of Semiconductors* (Springer-Verlag, Berlin, 1996).

[12] F. Vallée and F. Bogani, Phys. Rev. B **43**, 12 049 (1991).

[13] K. Turner, L. Rota, R. A. Taylor, J. F. Ryan, and C. T. Foxon, Appl. Phys. Lett. **66**, 3188 (1995).

[14] P. Langot, N. Del Fatti, D. Christofilos, R. Tommasi, and F. Vallée, Phys. Rev. B **54**, 14 487 (1996).

[15] T. Saito, O. Matsuda, and O. B. Wright, Phys. Rev. B **67**, 205421 (2003).

[16] V. Gusev, P. Picart, D. Mounier, and J. M. Breteau, Opt. Commun. **204**, 229 (2002).

[17] W. Gao, V. Gusev, C. Glorieux, J. Thoen, and B. Borghs, Opt. Commun. **143**, 19 (1997).

[18] H. Haken, *Quantum Field Theory of Solids–An Introduction* (North-Holland, Amsterdam, 1976).

[19] G. Bastard, *Wave Mechanics Applied to Semiconductor Heterostructures* (Halsted Press, New York, 1988).

[20] D. H. Hurley and O. B. Wright, Opt. Lett. **24**, 1305 (1999).

[21] O. B. Wright and V. E. Gusev, Appl. Phys. Lett. **66**, 1190 (1995).

[22] S. Adachi, *Properties of Aluminium Gallium Arsenide* (INSPEC, London, 1993).

[23] O. Matsuda and O. B. Wright, J. Opt. Soc. Am. B **19**, 3028 (2002).

[24] S. Adachi, *GaAs and Related Materials* (World Scientific, Singapore, 1994).

[25] S. Adachi, J. Appl. Phys. **58**, R1 (1985).

[26] G. Bastard, Phys. Rev. B **24**, 5693 (1981).

[27] D. Arnold, A. Ketterson, T. Henderson, J. Klem, and H. Morkoç, J. Appl. Phys. **57**, 2880 (1985).

[28] J. Batey and S. L. Wright, J. Appl. Phys. **59**, 200 (1986).

[29] W. Chen, H. J. Maris, Z. R. Wasilewski, and S. Tamura, Philos. Mag. B **70**, 687 (1994).

[30] O. Matsuda and O. B. Wright, Rev. Sci. Instrum. **74**, 895 (2003).

[31] The piezoelectric effect is not active in the experiments in the present investigation involving GaAs-based crystalline materials with (100) surface orientation.

[32] When cubic crystals such as GaAs are subjected to a hydrostatic pressure p, only longitudinal strain components are induced: $\eta_{xx} + \eta_{yy} + \eta_{zz} = 3\eta_{xx} = -(1/B)p$. The change in energy gap is determined by $\partial E_g / \partial p$ and by the hydrostatic deformation potential $\partial E_g / \partial \eta_{xx}$: $(\partial E_g / \partial p)p = (\partial E_g / \partial \eta_{xx})(\eta_{xx} + \eta_{yy} + \eta_{zz})$. Therefore, $\partial E_g / \partial \eta_{xx} = -B(\partial E_g / \partial p)$.

[33] These ratios of the carrier densities are 1:1 for QW1:QW2 at 1.50 eV and 1:2:1 for QW1:QW2:QW3 at 1.64 eV.

[34] This was calculated by converting the photoelastic constants P_{ij} reported by P. Etchegoin *et al.*, Phys. Rev. B **46**, 15 139 (1992) to those relevant here: $dN/d\eta_{zz} + idK/d\eta_{zz} = (P_{11}c_{12} + P_{12}c_{11} + P_{12}c_{12})/2(N+iK)$, where c_{11} and c_{12} are elastic constants taken from Ref. 24. A similar equation quoted for $dN/d\eta_{zz} + idK/d\eta_{zz}$ in Ref. 6 is in error.

[35] The frequency-squared ultrasonic attenuation tends to convert any strain pulse profile to a temporally Gaussian profile after propagation. This effect implies that the strain pulse becomes approximately Gaussian in shape after propagation by the ~300 nm separating the wells from the surface.